

# Nonlinear parameter-varying state-feedback design for a gyroscope using virtual control contraction metrics<sup>†</sup>

Ruigang Wang<sup>1</sup>, Patrick J.W. Koelwijn<sup>2</sup>, Ian R. Manchester<sup>1</sup>, Roland Tóth<sup>2</sup>

1. Australian Centre for Field Robotics & Sydney Institute for Robotics and Intelligent Systems,  
The University of Sydney, Sydney, NSW 2006, Australia

2. Department of Electrical Engineering, Eindhoven University of Technology, Eindhoven, The Netherlands

## SUMMARY

In this paper, we present a virtual control contraction metric (VCCM) based nonlinear parameter-varying (NPV) approach to design a state-feedback controller for a control moment gyroscope (CMG) to track a user-defined trajectory set. This VCCM based nonlinear stabilization and performance synthesis approach, which is similar to linear parameter-varying (LPV) control approaches, allows to achieve exact guarantees of exponential stability and  $\mathcal{L}_2$ -gain performance on nonlinear systems with respect to all trajectories from the predetermined set, which is not the case with the conventional LPV methods. Simulation and experimental studies conducted in both fully- and under-actuated operating modes of the CMG show effectiveness of this approach compared to standard LPV control methods. Copyright © 2020 John Wiley & Sons, Ltd.

Received ...

KEY WORDS: nonlinear parameter-varying, contraction, nonlinear system, stability

## 1. INTRODUCTION

With increasing performance expectations and growing complexity of engineered systems, it requires industrial control practice to achieve stabilization and shaping of the behavior of nonlinear dynamical systems. To address these problems, one possible methodology, which has seen rapid growth over the last few decades with many successful applications, is the so-called *linear parameter-varying* (LPV) approach. In the LPV framework, the behavior, i.e., solution set, of a nonlinear system is embedded in an LPV representation, which has a linear dynamic relation between its inputs and output [1]. This linear relation is dependent on a so-called *scheduling variable*, a function of the states, inputs and/or outputs, that represents the nonlinear dynamical aspects of the original nonlinear system. The scheduling variable is assumed to be measurable in the system. This idea has allowed the successful extension of many analysis and synthesis tools of the *linear time-invariant* (LTI) framework, such as the  $\mathcal{L}_2$ -gain stability and performance concept [2, 3, 4, 5], to provide convex analysis and controller synthesis for nonlinear systems through the LPV framework. More recently, extensions have been made to so-called *nonlinear parameter-varying* (NPV) systems, where some nonlinear dynamics are still included in the model allowing for a less conservative representation of the nonlinear system [6, 7, 8]. However, convex analysis

<sup>†</sup>This work has received funding from the Australian Research Council under the Discovery Project DP150100577 and the European Research Council (ERC) under the European Union's Horizon 2020 research and innovation programme (grant agreement nr. 714663).

and synthesis results are more difficult to obtain, due to the system not being linear, as is the case in the LPV framework.

While, the analysis and synthesis results of the LPV framework have successfully been applied in many engineering problems [9, 10], recent research has shown that naively applying these results to nonlinear systems can result in incorrect analysis results or unwanted closed-loop behavior in case of synthesis [11, 12, 13]. These issues stem from the fact that unlike LTI systems, stability properties of the origin and other forced equilibria are not equivalent for nonlinear systems. As a consequence, stability guarantees of an LPV/NPV embedding for the origin extend to that of the respective nonlinear model, but such guarantees are not sufficient to imply stability of all forced equilibria of the represented nonlinear system [13].

As it turns out, the loss of guarantees are attributed to the used equilibrium-dependent stability notion – widely applied in LPV control – raising the question if with a different equilibrium-free stability concept such problems could be avoided without losing the convexity and attractive properties of LPV approaches. As an alternative, the concept of *universal stabilization* aims to achieve exponential stability of all trajectories of the system [14]. By a so-called *control contraction metric* (CCM), analogous to the *control Lyapunov function* (CLF) for a single equilibrium (or trajectory) [15], convex conditions can be derived for analysis and synthesis under universal stabilization [16]. The ideas behind of these methods build on the concept of contraction analysis [17, 18], where analysis of convergence of the infinitesimal variations of the system around all trajectories (i.e., local stability of all trajectories) is equivalent with universal stability of the system (i.e., global stability of all trajectories). This leads to analysis and synthesis problems for a family of local linear systems, called *differential dynamics*, that can be elegantly expressed as an LPV system and solved by LPV synthesis tools to give exact stability and performance guarantees on the resulting closed-loop nonlinear system through the CCM approach.

While the use of CCM allows to achieve universal stability and performance with LPV control, it may be a too strict notion if stabilization of only a particular subset of reference trajectories is required, as is common in tracking control. Hence, the notion of  $\mathcal{B}^*$ -universal stabilizability has been introduced where stability of a subset of trajectories, denoted by  $\mathcal{B}^*$ , is aimed at, and which can be analyzed through so-called *virtual control contraction metrics* (VCCMs) [19]. The concept of VCCMs combines the notion of virtual systems [20] and CCMs. An earlier work of virtual contraction theory in control design can be found in [21]. Some recent works include control synthesis for a special case of mechanical systems [22] and further extension to port-Hamiltonian systems [23]. The main idea of virtual systems is that a nonlinear system, which is not itself contracting, may have weaker stability properties that can be established via construction of an auxiliary (virtual) system which is contracting. Furthermore, the virtual system can be seen as a NPV embedding of the dynamics of the original system. Then, its differential dynamics can be still expressed as an LPV system, which allows the use of convex LPV synthesis results through the CCM approach, but with extended feasibility due to the reduced conservativeness of the embedding. The VCCM based control approach can achieve  $\mathcal{B}^*$ -universal stabilization and  $\mathcal{L}_2$ -gain performance guarantees for nonlinear systems. In contrast to the reference-dependent variable-gain tracking control approaches for linear systems [24, 25], the VCCM approach can deal with nonlinear systems and yield controllers whose gain depends on both states and references.

In this paper the VCCM based controller design is applied in order to achieve  $\mathcal{B}^*$ -universal stabilizability and performance shaping for a *control moment gyroscope* (CMG). CMGs have been widely applied in attitude control of ships [26], satellites [27], and the international space station [28]. They represent a challenging nonlinear system and are often used for the demonstration of nonlinear control methods [29, 30]. Two control configurations (fully- and under-actuated modes) of the CMG are considered. Furthermore, the influence of the used LPV or NPV embedding for the CMG on the achieved controller performance is investigated by constructing controllers using both type of embeddings in the VCCM based controller design approach. The simulation and experimental studies show how the choice of embedding model and control realization affects the closed-loop tracking performance. This type of question is not well-addressed in the LPV literature. The comparison results show that the NPV approach can ensure closed-loop stability

and performance for user-specified tracking tasks while the conventional LPV approach may not provide such guarantees.

The paper is structured as follows. In Section 2, a formal problem formulation is given, along with a description of the considered dynamical model for the CMG. Section 3 describes the VCCM based controller design for NPV embeddings. In Section 5, a simulation study is presented for the CMG using the introduced controller design methods and the results are thoroughly analyzed both from the view point of stability and achieved performance. Finally, in Section 6, concluding remarks on the presented work are given.

### Notation

$\mathbb{R}$  is the set of real numbers, while  $\mathbb{R}_+$  is the set of non-negative reals. Let  $(x, y)$  denote the vector concatenation of  $x \in \mathbb{R}^n$ ,  $y \in \mathbb{R}^m$ , i.e.,  $(x, y) := [x^\top y^\top]^\top \in \mathbb{R}^{n+m}$ .  $\mathcal{L}_2$  is the space of square-integrable vector signals on  $\mathbb{R}_+$ , i.e.,  $\|x\|_2 := \sqrt{\int_0^\infty |x(t)|^2 dt} < \infty$  where  $|\cdot|$  is the Euclidean norm. The causal truncation  $(\cdot)_T$  is defined by  $(x)_T(t) := x(t)$  for  $t \in [0, T]$  and 0 otherwise.  $\mathcal{L}_2^c$  is the space of vector signals on  $\mathbb{R}_+$  whose causal truncation belongs to  $\mathcal{L}_2$ . For a matrix  $A$ ,  $A \succ 0$  or  $A \succeq 0$  means that  $A$  is positive definite or positive semi-definite. Similarly  $A \prec 0$  or  $A \preceq 0$  means that  $A$  is negative definite or negative semi-definite. A Riemannian metric is a smooth matrix function  $M : \mathbb{R}^n \rightarrow \mathbb{R}^{n \times n}$  with  $M(x) \succ 0$  for all  $x \in \mathbb{R}^n$ . A metric  $M(x)$  is said to be uniformly-bounded if there exist  $a_2 \geq a_1 > 0$  such that  $a_1 I \succeq M(x) \succeq a_2 I$  for all  $x \in \mathbb{R}^n$ . Let  $\gamma(x_0, x_1)$  be the set of smooth paths connecting  $x_0$  to  $x_1$ , that is, each  $c \in \Gamma(x_0, x_1)$  is a smooth map  $c : [0, 1] \rightarrow \mathbb{R}^n$  with  $c(0) = x_0$  and  $c(1) = x_1$ . Given a metric  $M(x)$ , a geodesic  $\gamma$  is a (non-unique) minimum length path defined by  $\gamma := \arg \inf_{c \in \Gamma(x_0, x_1)} \mathcal{E}(c)$  where  $\mathcal{E}(c) := \int_0^1 c_s^\top M(c(s)) c_s ds$ . If  $M$  is independent of  $x$ , then  $\gamma$  is the straight line  $\gamma(s) = (1-s)x_0 + sx_1$ .

## 2. PROBLEM FORMULATION

In this paper, we consider a 3-DOF CMG, see Figure 1(a), consisting of three gimbals (A, B and C) along with a symmetric disk (D), called the fly-wheel. The configuration of the CMG is depicted in Figure 1(b). Let  $q = (q_1, q_2, q_3, q_4)$  be the generalized angular position vector and  $i = (i_1, i_2, i_3, i_4)$  be the motor currents vector. Here the index  $j = 1, 2, 3, 4$  refers to the frame D, C, B, A, respectively. The dynamics of the gyroscope can be represented by ([31, 32])

$$H(q)\ddot{q} + [C(q, \dot{q}) + F_v]\dot{q} = K_m i, \quad (1)$$

where  $F_v = \text{diag}(f_v)$  with  $f_v$  as the viscous friction vector,  $K_m = \text{diag}(k_m)$  with  $k_m$  as the motor constant vector. The inertia matrix is given as  $H(q) = \sum_{k \in \mathcal{S}} H_k(q_2, q_3)$  where the inertia matrices for each frame in  $\mathcal{S} = \{A, B, C, D\}$  are listed as follows:

$$\begin{aligned} H_A &= \begin{bmatrix} 0 & 0 & 0 & 0 \\ \star & 0 & 0 & 0 \\ \star & \star & 0 & 0 \\ \star & \star & \star & K_A \end{bmatrix}, & H_B &= \begin{bmatrix} 0 & 0 & 0 & 0 \\ \star & 0 & 0 & 0 \\ \star & \star & J_B & 0 \\ \star & \star & \star & I_B s_3^2 + K_B c_3^2 \end{bmatrix}, \\ H_C &= \begin{bmatrix} 0 & 0 & 0 & 0 \\ \star & I_C & 0 & -I_C s_3 \\ \star & \star & J_C c_2^2 + K_C s_2^2 & \alpha_1 s_2 c_2 c_3 \\ \star & \star & \star & I_C s_3^2 + (J_C s_2^2 + K_C c_2^2) c_3^2 \end{bmatrix}, \\ H_D &= \begin{bmatrix} J_D & 0 & J_D c_2 & J_D s_2 c_3 \\ \star & I_D & 0 & -I_D s_3 \\ \star & \star & I_D s_2^2 + J_D c_2^2 & \alpha_2 s_2 c_2 c_3 \\ \star & \star & \star & I_D s_3^2 + (I_D c_2^2 + J_D s_2^2) c_3^2 \end{bmatrix}, \end{aligned}$$

with  $\alpha_1 = J_C - K_C$  and  $\alpha_2 = J_D - I_D$ . For compactness and readability, sinusoidal functions are abbreviated as  $s_i$  and  $c_i$ , e.g.,  $\sin q_2 = s_2$  and  $\cos^2 q_3 = c_3^2$ . The terms  $I_k, J_k, K_k$  with  $k \in \mathcal{S}$  are the

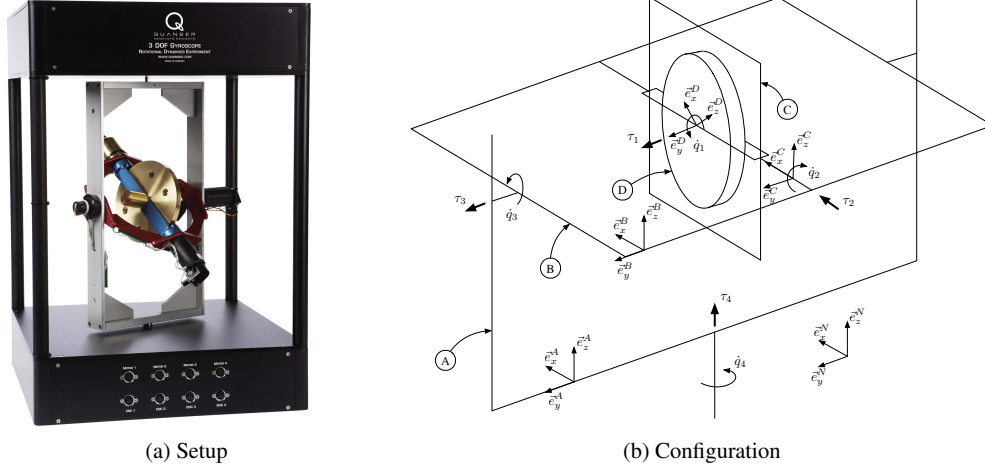


Figure 1. 3-DOF CMG.

scalar moments of inertia about the  $x$ ,  $y$ ,  $z$  axes respectively in the bodies  $k$ . The symbol  $\star$  denotes terms required to make the matrix symmetric.

The elements of the Coriolis matrix  $C(q, \dot{q})$  can be computed as:

$$C(q, \dot{q}) = \begin{bmatrix} \dot{q}^\top & 0 & 0 & 0 \\ 0 & \dot{q}^\top & 0 & 0 \\ 0 & 0 & \dot{q}^\top & 0 \\ 0 & 0 & 0 & \dot{q}^\top \end{bmatrix} \begin{bmatrix} \Gamma^1(q) \\ \Gamma^2(q) \\ \Gamma^3(q) \\ \Gamma^4(q) \end{bmatrix}, \quad (2)$$

where

$$\Gamma^1 = \frac{1}{2} \begin{bmatrix} 0 & 0 & 0 & 0 \\ \star & 0 & -J_D s_2 & J_D c_2 c_3 \\ \star & \star & 0 & -J_D s_2 s_3 \\ \star & \star & \star & 0 \end{bmatrix}, \quad \Gamma^2 = \frac{1}{2} \begin{bmatrix} 0 & 0 & J_D s_2 & -J_D c_2 c_3 \\ \star & 0 & 0 & 0 \\ \star & \star & -2\alpha_3 s_2 c_2 & \alpha_3 (c_2^2 c_3 - s_2^2 c_3) - \alpha_4 c_3 \\ \star & \star & \star & \alpha_3 c_2 c_3^2 s_2 \end{bmatrix},$$

$$\Gamma^3 = \frac{1}{2} \begin{bmatrix} 0 & -J_D s_2 & 0 & J_D s_2 s_3 \\ \star & 0 & 2\alpha_3 s_2 c_2 & \alpha_4 c_3 + \alpha_3 (c_3 s_2^2 - c_2^2 c_3) \\ \star & \star & 0 & 0 \\ \star & \star & \star & -(\alpha_5 + \alpha_3 s_2^2) c_3 s_3 \end{bmatrix},$$

$$\Gamma^4 = \frac{1}{2} \begin{bmatrix} 0 & J_D c_2 c_3 & -J_D s_2 s_3 & 0 \\ \star & 0 & \alpha_3 (c_3 s_2^2 - c_2^2 c_3) - \alpha_4 c_3 & -\alpha_3 c_2 c_3^2 s_2 \\ \star & \star & \alpha_3 c_2 s_2 s_3 & (\alpha_5 + \alpha_3 s_2^2) c_3 s_3 \\ \star & \star & \star & 0 \end{bmatrix},$$

with  $\alpha_3 = I_D - J_C - J_D + K_C$ ,  $\alpha_4 = I_C + I_D$  and  $\alpha_5 = I_B + I_C - K_B - K_C$ . The physical parameters of the gyroscope are given in the Table I. Here we are interested in tracking control for the following two operating modes:

- OM-1: The gimbal A is locked, i.e.  $(q_4, \dot{q}_4) = 0$  and  $i_4 = 0$ . The control objective is to track a set of reference signals of  $\dot{q}_1, \dot{q}_2$  and  $\dot{q}_3$  using the input  $(i_1, i_2, i_3)$ .
- OM-2: The gimbal B is locked, i.e.  $(q_3, \dot{q}_3) = 0$  and  $i_3 = 0$ . The control objective is set-point tracking for  $\dot{q}_1$  and  $\dot{q}_4$  by using the input  $(i_1, i_2)$ . In this case, the motor on gimbal A is switched off, i.e.  $i_4 = 0$ , and hence the system is underactuated.

Note that OM-1 is relatively easy to control as the CMG is fully-actuated. For OM-2, control design is a challenging task as the dynamics is highly nonlinear and under-actuated.

Table I. Model parameters of CMG.

Index		Moments			Index		Constants	
$k$	$I$	$J$	$K$	$i$	$f_v$	$k_m$		
A	0.0902	0.0534	0.0374	1	$1.1050 \times 10^{-5}$	0.0680		
B	0.0039	0.0186	0.0200	2	$1.2420 \times 10^{-5}$	0.1006		
C	$9.2087 \times 10^{-4}$	0.0016	0.0026	3	0.0141	0.1053		
D	0.0030	0.0055	0.0374	4	0.0327	0.0606		

### 3. PARAMETER-VARYING EMBEDDINGS AND VIRTUAL CONTROL CONTRACTION METRICS

#### 3.1. Control via NPV embedding

Consider nonlinear (NL) systems of the form

$$\dot{x} = f(x, u), \quad (3)$$

where  $x(t) \in \mathbb{X} \subseteq \mathbb{R}^n$  is the measured state and  $u(t) \in \mathbb{U} \subseteq \mathbb{R}^m$  is the control input. The function  $f$  is assumed to be sufficiently smooth. We define a *reference trajectory*  $(x^*, u^*)$  to be a forward-complete solution of (3). A reference trajectory is said to be globally exponentially stabilizable if there exist a state feedback controller of the form

$$u = \kappa(x, x^*, u^*), \quad (4)$$

where  $\kappa : \mathbb{X} \times \mathbb{X} \times \mathbb{U} \rightarrow \mathbb{U}$  such that the closed-loop (CL) system  $\dot{x} = f(x, \kappa(x, x^*, u^*))$  is globally exponentially stable at  $(x^*, u^*)$ , i.e.,

$$|x(t) - x^*(t)| \leq R e^{-\lambda t} |x(0) - x^*(0)|, \quad \forall t > 0, \quad (5)$$

for some constants  $\lambda, R > 0$ .

We will present a systematic approach to design controllers of the form (4) that achieve globally exponential stability for any reference trajectory  $(x^*, u^*)$  from a user-defined set  $\mathcal{B}^*$ . If such controllers exist, we call system (3)  *$\mathcal{B}^*$ -universally stabilizable*. Furthermore, if  $\mathcal{B}^*$  contains all reference trajectories, we simply call (3) *universally stabilizable*. Note that depending on the choice of  $\mathcal{B}^*$ , the task could be regulation, set-point tracking or reference tracking.

In this work, we will first construct a *virtual system* for (3), which is a new system of the form:

$$\dot{\chi} = F(\chi, x, \mu), \quad (6)$$

with the property of  $F(x, x, u) = f(x, u)$ ,  $\forall (x, u) \in \mathbb{X} \times \mathbb{U}$ , where the virtual state  $\chi(t) \in \mathbb{X}$  and the virtual input  $\mu(t) \in \mathbb{U}$  live in a copy of the state/input spaces of (3), and the external variable  $x(t)$  is taken as the state of (3). Note that the virtual system (6) can also be understood as a nonlinear parameter-varying (NPV) embedding of (3) since the behavior (solution set) of (3) can be embedded into the behavior of (6) via the map  $F$ , which is called the *behavior embedding principle*. The control design based on behavior embedding principle usually includes three steps: the choice of a NPV model (6), the control synthesis based on it and the realization of the controller for the original system (3).

Note that the NPV embedding (6) is not unique as there are various choices in terms of what level of nonlinearity is “hidden” in the external parameter. For example, the linear parameter-varying (LPV) form ([1, 10]) is an embedding where  $F$  is linear in  $\chi$  and  $\mu$ . Furthermore, the system (3) is a trivial embedding of itself when the full nonlinearity is considered. Note that an LPV embedding allows for simpler control synthesis but may lead to conservative results. Compared to the linear (standard LPV) case, some recent works [8] show that the performance can be improved by considering certain level of system nonlinearity. Here we construct the NPV embedding (6) such that the following two conditions are satisfied:

**C1)** For any trajectory  $x$  of system (3), the virtual system (6) can be universally stabilized by a controller of the form

$$\mu = \mu^* + \kappa^{\text{fb}}(\chi, \chi^*, x), \quad (7)$$

with  $\kappa^{\text{fb}} : \mathbb{X} \times \mathbb{X} \times \mathbb{X} \rightarrow \mathbb{U}$  and  $\kappa^{\text{fb}}(\chi^*, \chi^*, x) = 0, \forall \chi^*, x \in \mathbb{X}$ , where  $(\chi^*, x, \mu^*)$  is an admissible trajectory of (6).

**C2)** There exists a controller  $\kappa^{\text{ff}} : \mathbb{X} \times \mathbb{X} \times \mathbb{U} \rightarrow \mathbb{U}$  such that for any reference trajectory  $(x^*, u^*) \in \mathcal{B}^*$  and any trajectory  $x$  of system (3),  $(x^*, x, \mu^*)$  is a feasible solution to (6), where the feed-forward input  $\mu^*$  is given by

$$\mu^* = \kappa^{\text{ff}}(x, x^*, u^*). \quad (8)$$

The following theorem gives a NPV controller that achieves  $\mathcal{B}^*$ -universal stability for (3).

*Theorem 1 ([19])*

Consider the NL system (3) and a reference set  $\mathcal{B}^*$ . If there exists a NPV embedding (6) such that Conditions **C1** and **C2** hold, then (3) is  $\mathcal{B}^*$ -universally stable under the controller

$$u = \kappa^{\text{ff}}(x, x^*, u^*) + \kappa^{\text{fb}}(x, x^*, x). \quad (9)$$

*Proof*

Note that the above theorem is a special case of [19, Thm. 2]. Here we give a sketch proof as follows. By Condition **C2** and the behavior embedding principle, the trajectories  $(x^*, x, \mu^*)$  and  $(x, x, u)$  with  $u$  given in (9) are two solutions of the CL virtual system of (6) and (7). Then,  $x(t)$  converges to  $x^*(t)$  exponentially as the CL system is contracting according to Condition **C1**.  $\square$

Note that the NPV controller (9) contains two parts: a feedback term that achieves universal stability for the NPV system and a feed-forward term that ensures any  $x^*$  from  $\mathcal{B}^*$  is admissible to the NPV embedding for all possible  $x$ . Note that the universal stability notion used in Condition **C1** is much stronger than the standard stability concept. Under this strong notion, control synthesis for NPV systems can have a convex formulation similar to the LPV approach, as shown in the next section. The necessity of Condition **C2** for CL stability guarantees will be discussed in Section 3.4.

### 3.2. VCCM based control design

This section presents a constructive approach [19] to the universal stabilization problem in Condition **C1**. For any fixed exogenous signal  $x$  generated by the original NL dynamics (3), the virtual system (6) becomes a time-varying NL system, we can then apply the CCM-based method [14] to design a universally stabilizing controller. In this approach, one considers a prolonged system consisting of (6) and its differential dynamics:

$$\dot{\delta}_\chi = A(\chi, x, \mu)\delta_\chi + B(\chi, x, \mu)\delta_\mu := \frac{\partial F(\chi, x, \mu)}{\partial \chi}\delta_\chi + \frac{\partial F(\chi, x, \mu)}{\partial \mu}\delta_\mu, \quad (10)$$

defined along solutions  $(\chi, \mu)$ . Here  $(\delta_\chi, \delta_\mu)$  represents the infinitesimal variations between  $(\chi, \mu)$  and its neighborhood solutions. Note that we do not include variation on  $x$  as it only needs to consider the contraction property of all virtual state trajectories  $\chi$  which are generated under the same exogenous signal  $x$ . In this differential setting, many existing tools from the linear system theory (e.g. LMI based control design) can be applied.

A *virtual control contraction metric* (VCCM)  $M(\chi, x)$  is a uniformly bounded matrix function  $M : \mathbb{X} \times \mathbb{X} \rightarrow \mathbb{R}^{n \times n}$  (i.e., there exist some  $a_2 \geq a_1 > 0$  such that  $a_1 I \preceq M(\chi, x) \preceq a_2 I$  for all  $\chi, x$ ) such that the following implication is true for all  $(\chi, x, \mu) \in \mathbb{X} \times \mathbb{X} \times \mathbb{U}$ :

$$\delta_\chi \neq 0, \delta_\chi^\top M B = 0 \Rightarrow \delta_\chi^\top (\dot{M} + A^\top M + M A + 2\lambda M)\delta_\chi < 0. \quad (11)$$

The existence of a VCCM implies that (6) is universally stabilizable [14]. Furthermore, we can find a dual metric  $W = M^{-1}$  and a matrix function  $Y(\chi, x) \in \mathbb{R}^{m \times n}$  satisfying

$$-\dot{W} + AW + WA^\top + BY + Y^\top B^\top + 2\lambda W \preceq 0 \quad (12)$$



for all  $(\chi, x, \mu) \in \mathbb{X} \times \mathbb{X} \times \mathbb{U}$ . Note that the above formulation is convex, but infinite dimensional, as the decision variables  $M, Y$  are smooth matrix functions. Finite-dimensional LMI approximations include LPV synthesis techniques [1] or sum-of-squares relaxation [33]. The pointwise LMI (12) yields a differential state-feedback controller

$$\delta_\mu = K(\chi, x)\delta_\chi := Y(\chi, x)W^{-1}(\chi, x)\delta_\chi. \quad (13)$$

Note that the above differential controller design can be treated as LPV synthesis problem since the differential dynamics satisfies the properties of an LPV system [34].

The realization task is to construct a controller satisfying Condition **C1** from the differential gain  $K$ . One solution is the path integral based realization [14] of the local LPV controller (13):

$$\mu = \mu^* + \underbrace{\int_0^1 K(\gamma(s), x)\gamma_s(s)ds}_{\kappa^{\text{fb}}(\chi, \chi^*, x)} \quad (14)$$

where  $\gamma$  is a geodesic connecting  $\chi^*$  to  $\chi$  with respect to the metric  $M(\chi, x) = W^{-1}(\chi, x)$ . The above realization satisfies  $\kappa^{\text{fb}}(\chi^*, \chi^*, x) = 0$ ,  $\forall \chi^*, x \in \mathbb{X}$  and  $\mu_s = K(\gamma(s), x)\gamma_s$ , that is, it is an exact realization of (13) with  $\delta_\mu = \mu_s$  and  $\delta_\chi = \gamma_s$  along the path  $\gamma$ .

The realization (14) has an LPV interpretation as follows. First, we take sufficiently many sample points of the path  $\gamma$  (i.e.  $0 = s_0 < s_1 < \dots < s_N = 1$ ) such that  $\gamma(s_{i+1}) - \gamma(s_i) \approx \gamma_s(s_i)\Delta s_i$  where  $\Delta s_i = s_{i+1} - s_i$ , as shown in Figure 2. Then, we can define a control sequence for those points by

$$\nu(s_{i+1}) = \nu(s_i) + K(\gamma(s_i), x)\gamma_s(s_i)\Delta s_i = \nu(s_i) + K(\gamma(s_i), x)(\gamma(s_{i+1}) - \gamma(s_i)) \quad (15)$$

with  $\nu(s_0) = \mu^*$ . This can be understood as a series of local LPV controllers where each control action  $\nu(s_{i+1})$  tries to make  $\gamma(s_{i+1})$  exponentially converge to  $\gamma(s_i)$ . Thus, it also makes  $\gamma(s_{i+1})$  exponentially converges to the reference point  $\chi^* = \gamma(s_0)$ . When the number of intermediate states approaches infinity at each sampling point  $t$ , the sequence (15) becomes a smooth control path  $\nu : [0, 1] \rightarrow \mathbb{U}$  defined as the path integral of local LPV controller (13):

$$\nu(s) := \mu^* + \int_0^s K(\gamma(\mathfrak{s}), x)\gamma_s(\mathfrak{s})d\mathfrak{s}. \quad (16)$$

The controller (14) is the end point of this path, i.e.  $\mu = \nu(1)$ . If  $M, K$  are independent of  $\chi$  and  $\mu$  respectively, we can obtain an explicit controller of the form

$$\mu = \mu^* + \left[ \int_0^1 K(\tilde{\chi}(s), x)ds \right] (\chi - \chi^*), \quad (17)$$

where  $\tilde{\chi}(s) = \chi^* + s(\chi - \chi^*)$ . For the general case where  $M$  is  $\chi$ -dependent, the controller (14) usually requires solving an online optimization problem to construct a geodesic. For fast-sampling applications, there exist some real-time approximation methods, e.g. pseudo-spectral method [35] and gradient flows [36].

### 3.3. Performance design

We will also consider the performance design for the  $\mathcal{B}^*$ -specified tracking problem under load disturbance such as additive friction offsets, imbalance etc. As shown in Figure 3, the performance outputs of state error and control effort are defined by  $z_1 = W_1(x - x^*)$  and  $z_2 = W_2(u - u^*)$ , respectively, where  $W_1, W_2$  are stable linear weighting filters. With minor abuse of notation, we use  $x$  to refer to the state of the augmented system consisting of  $G, W_1$  and  $W_2$ . The augmented system can be represented by the following general form

$$\dot{x} = f(x, u, d), \quad z = h(x, u, d), \quad (18)$$

where  $z = (z_1, z_2)$ . Applying the controller (4) to (18) yields the CL system

$$\dot{x} = f(x, \kappa(x, x^*, u^*), d), \quad z = h(x, \kappa(x, x^*, u^*), d). \quad (19)$$

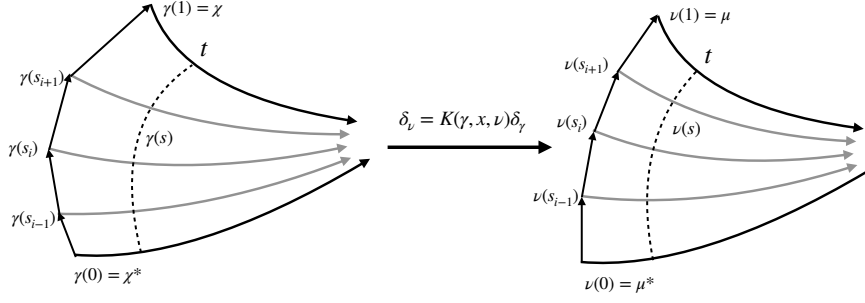


Figure 2. An LPV interpretation of the path integral based realization.

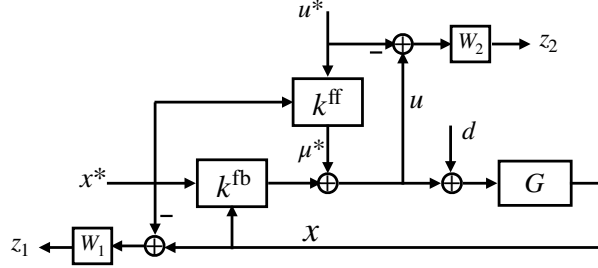


Figure 3. Diagram for the NPV based performance design.

### Definition 1

The CL system (19) is said to achieve  $\mathcal{L}_2$ -gain bound of  $\alpha$  at  $(x^*, u^*, d^*, z^*)$  if for all  $T > 0$

$$\|z - z^*\|_T^2 \leq \alpha^2 \|d - d^*\|_T^2 + \beta(x(0), x^*(0)), \quad (20)$$

for some function  $\beta(x_1, x_2) \geq 0$  with  $\beta(x, x) = 0$ , where  $d^* = 0$ ,  $z^* = 0$  are the nominal values of the disturbance and performance output, respectively. The controlled system (19) is said to have a  $\mathcal{B}^*$ -universal  $\mathcal{L}_2$ -gain bound of  $\alpha$ , if (20) holds for all reference trajectories  $(x^*, u^*) \in \mathcal{B}^*$ . If  $\mathcal{B}^*$  is the set of all feasible reference trajectories, we simply call (19) universal  $\mathcal{L}_2$ -gain bounded by  $\alpha$ .

Note that the  $\mathcal{B}^*$ -universal gain condition (20) is stronger than the standard  $\mathcal{L}_2$ -gain bound, but weaker than the incremental  $\mathcal{L}_2$  gain bound [16]. To extend the NPV approach for the disturbance rejection problem, we first construct a NPV virtual system of the form

$$\dot{\chi} = F(\chi, x, \mu, d), \quad \zeta = H(\chi, x, \mu, d), \quad (21)$$

where  $\chi(t), \mu(t), \zeta(t)$  live in the same spaces as  $x(t), u(t), z(t)$ , respectively. From the NPV embedding principle, we have  $F(x, x, u, d) = f(x, u, d)$  and  $H(x, x, u, d) = h(x, u, d)$ .

The associated differential dynamics of (21) is

$$\begin{aligned} \dot{\delta}_\chi &= A(\sigma)\delta_\chi + B(\sigma)\delta_\mu + B_d(\sigma)\delta_d, \\ \dot{\delta}_\zeta &= C(\sigma)\delta_\chi + D(\sigma)\delta_\mu + D_d(\sigma)\delta_d, \end{aligned} \quad (22)$$

where  $\sigma = (\chi, x, \mu, d)$ ,  $A = \frac{\partial F}{\partial \chi}$ ,  $B = \frac{\partial F}{\partial \mu}$ ,  $B_d = \frac{\partial F}{\partial d}$ ,  $C = \frac{\partial H}{\partial \chi}$ ,  $D = \frac{\partial H}{\partial \mu}$  and  $D_d = \frac{\partial H}{\partial d}$ . Applying the differential state feedback (13) to (22) gives the CL differential dynamics:

$$\begin{aligned} \dot{\delta}_\chi &= (A + BK)\delta_\chi + B_d\delta_d, \\ \dot{\delta}_\zeta &= (C + DK)\delta_\chi + D_d\delta_d. \end{aligned} \quad (23)$$

To establish an  $\mathcal{L}_2$ -gain bound for (23), the choice of VCCM is a uniformly bounded metric  $M(\chi, x)$ , satisfying

$$\dot{V}(\chi, x, \delta_\chi) \leq -\frac{1}{\alpha} |\delta_\zeta|^2 + \alpha |\delta_d|^2, \quad (24)$$



where  $V(\chi, x, \delta_\chi) = \delta_\chi^\top M(\chi, x) \delta_\chi$  can be interpreted as a differential storage function. Integration of the above dissipation condition along the geodesics gives the universal  $\mathcal{L}_2$ -gain bound of  $\alpha$  [16].

Similar to the case of  $H_\infty$  state-feedback control for linear systems (e.g., [37]), the condition (24) can be converted into the following pointwise LMI:

$$\begin{bmatrix} \mathcal{W} & B_d & (CW + DY)^\top \\ B_d^\top & -\alpha I & D_d^\top \\ (CW + DY) & D_d & -\alpha I \end{bmatrix} \prec 0, \quad (25)$$

where  $W = M^{-1}$ ,  $Y = KW$  and  $\mathcal{W} = -\dot{W} + AW + WA^\top + BY + Y^\top B^\top$ . Note that the above formulation is infinite dimensional but convex in  $W$  and  $Y$ . The finite-dimensional approximation techniques for (12) can also be applied here.

From [16, Th. 1] and the behavior embedding principle, the CL system (19) achieves an  $\mathcal{L}_2$ -gain bound of  $\alpha$  from  $d - d^*$  to  $z - \zeta^*$  where  $\zeta^* = H(x^*, x, \kappa^{\text{ff}}(x, x^*, u^*), d^*)$  satisfies  $\zeta^* = z^*$  if  $x = x^*$ . If there exists a constant  $\alpha_1 > 0$  such that  $|\zeta^* - z^*| \leq \alpha_1 |x - x^*|$ , we can obtain the  $\mathcal{L}_2$ -gain bound from  $d - d^*$  to  $\zeta^* - z^*$  as  $\alpha_1 \alpha_2$  where  $\alpha_2$  is the  $\mathcal{L}_2$ -gain bound from  $\delta_d$  to  $\delta_\chi$  of (23) with  $K = YW^{-1}$ . Then, the performance bound from  $d - d^*$  to  $z - z^*$  is given as follows.

*Theorem 2* ([19])

Consider the system (18) and its NPV embedding (21). Assume that the LMI (25) is feasible and Condition **C2** holds for (21) and the reference set  $\mathcal{B}^*$ . Then, the controller (9) achieves a  $\mathcal{B}^*$ -universal  $\mathcal{L}_2$ -gain bound of  $\tilde{\alpha} = \sqrt{\alpha^2 + (\alpha_1 \alpha_2)^2}$ .

*Remark 1*

When  $d = d^*$ , the tracking cost  $J_T(x_0, x_0^*) := \int_0^T |z(t)|^2 dt$  is bounded by

$$J_T(x_0, x_0^*) \leq J_\infty(x_0, x_0^*) \leq \alpha^2 \mathcal{E}(\gamma), \quad (26)$$

where  $\gamma$  is a geodesic joining  $x_0^*$  to  $x_0$ .

### 3.4. Comparison with the LPV embedding approach

In LPV based state-feedback control, system (3) is rewritten into an LPV embedding of the form

$$\dot{x} = \widehat{A}(\sigma)x + \widehat{B}(\sigma)u, \quad (27)$$

where  $\sigma = \phi(x)$  is the scheduling variable such that  $\widehat{A}(\phi(x))x + \widehat{B}(\phi(x))u = f(x, u)$ . Note that this embedding can be understood as an LPV virtual system as follows:

$$\dot{\chi} = A(x)\chi + B(x)\mu \quad (28)$$

with  $A(x) = \widehat{A}(\phi(x))$  and  $B(x) = \widehat{B}(\phi(x))$ . Since the virtual system is linear in  $\chi$  and  $\mu$ , we can use the VCCM based synthesis formulation (12) to construct an LPV controller  $\mu = K(x)\chi$  such that the CL system  $\dot{\chi} = A_c(x)\chi := [A(x) + B(x)K(x)]\chi$  is exponentially stable with respect to a Lyapunov function  $V(\chi) = \chi^\top M(x)\chi$ .

The standard LPV realization for reference tracking takes the form of

$$u = u^* + K(x)(x - x^*), \quad (29)$$

where  $(x^*, u^*)$  is a feasible solution of (3). The VCCM approach uses a different realization, denoted as LPV-VCCM controller, which has the form of

$$u = \kappa^{\text{ff}}(x, x^*, u^*) + K(x)(x - x^*), \quad (30)$$

where the feed-forward term  $\kappa$  satisfies Condition **C2**, i.e.,  $\dot{x}^* = A(x)x^* + B(x)\kappa^{\text{ff}}(x, x^*, u^*)$ . Note that when  $x^*$  is the origin, the standard LPV and LPV-VCCM controllers have the same realization as  $u = K(x)x$ . For general cases, they are not identical, resulting in different CL behaviors. Stability

of the VCCM-LPV approach can be rigorously guaranteed by Theorem 1 while the standard LPV controller may not offer such guarantees [11, 12, 13].

Here we give a brief explanation for the loss of stability guarantees of the standard LPV controller, see [19, Section 5.2] for details. From (28) - (29), we can derive the error dynamics as follows

$$\begin{aligned}\dot{e} &= A(x)x + B(x)[u^* + K(x)(x - x^*)] - A(x^*)x^* - B(x^*)u^* \\ &= A_c(x)e + [A(x) - A(x^*)]x^* + [B(x) - B(x^*)]u^* = [A_c(x) + \Delta(x, x^*, u^*)]e,\end{aligned}$$

where  $e := x - x^*$  and

$$\Delta(x, x^*, u^*)(x - x^*) = [A(x) - A(x^*)]x^* + [B(x) - B(x^*)]u^*. \quad (31)$$

Note that the term  $\Delta$  vanishes when  $x^*$  is the origin, otherwise it is generally non-zero. Now we look into the time derive of the Lyapunov function  $V(e) = e^\top M(x)e$ :

$$\dot{V}(e) = e^\top Qe + e^\top (\Delta^\top M + M\Delta)e, \quad (32)$$

where  $Q = \dot{M} + MA_c + A_cM \preceq -2\lambda M$ . When  $\Delta$  is sufficiently large, a smaller converge rate or even instability can be observed, see the academic example in [19, Section 5.2.2]. The above analysis also applies to the performance design where the bound (26) may not hold if Condition C2 is not satisfied. The VCCM approach can provide stability and performance guarantees since the feed-forward term  $\kappa^{\text{ff}}$  satisfying Condition C2 also ensures  $\Delta(x, x^*, u^*) \equiv 0$ .

## 4. CONTROL DESIGN FOR CMG

### 4.1. Fully-actuated operating mode: OM-1

Since the outer-most gimbal A is locked in this mode (i.e.,  $(q_4, \dot{q}_4) = 0$  and  $i_4 = 0$ ), we only need to take into account part of the CMG dynamics whose state and input are  $x = (q_2, q_3, \dot{q}_1, \dot{q}_2, \dot{q}_3)$  and  $u = (i_1, i_2, i_3)$ , respectively. The fly-wheel angle  $q_1$  can be ignored since it does not directly affects the dynamics of other states. Then, the state-space model of OM-1 can be written as follows

$$\dot{x} = A(x_1, x_2)x + B(x_1)u := \begin{bmatrix} 0 & E \\ 0 & \mathcal{H}(x_1)^{-1}(\mathcal{C}(x_1, x_2) + \mathcal{F}_v) \end{bmatrix} \begin{bmatrix} x_1 \\ x_2 \end{bmatrix} + \begin{bmatrix} 0 \\ \mathcal{H}(x_1)^{-1}\mathcal{K}_m \end{bmatrix} u, \quad (33)$$

where  $x = (x_1, x_2)$ ,  $x_1 = (q_2, q_3)$ ,  $x_2 = (\dot{q}_1, \dot{q}_2, \dot{q}_3)$  and  $E = [0 \ I]$ . Here  $\mathcal{H}, \mathcal{C}, \mathcal{F}_v, \mathcal{K}_m$  are constructed by eliminating the 4th row and column of the matrices  $H, C, F_v, K_m$  in (1), respectively. Note that the above dynamics are fully-actuated. For performance design, we consider the following perturbed dynamics:

$$\dot{x} = A(x_1, x_2)x + B(x_1)u + Dd, \quad z = \begin{bmatrix} W_1(x - x^*) \\ W_2(u - u^*) \end{bmatrix}, \quad (34)$$

with  $D = [0 \ I]^\top \in \mathbb{R}^{5 \times 3}$ , where  $d(t) \in \mathbb{R}^3$  is the input perturbation and the weighting matrices is chosen as  $W_1 = 1, W_2 = 0.2$ .

Here we only present the details about Lyapunov design as the performance design has the same procedure except solving a different point-wise LMI.

**Standard LPV control.** We consider the following LPV virtual system of (33):

$$\dot{\chi} = A(x_1, x_2)\chi + B(x_1)\mu \quad (35)$$

where the scheduling variables satisfy  $q_2, q_3 \in [-\frac{\pi}{3}, \frac{\pi}{3}]$ ,  $\dot{q}_1 \in [30, 60]$  and  $\dot{q}_2, \dot{q}_3 \in [-1, 1]$ . For Lyapunov design, the pointwise LMI (12) is solved by the grid-based method [38] with  $\lambda = 0.5$  and constant dual metric  $W$ . To be specific, the grid based approach approximates the LPV embedding

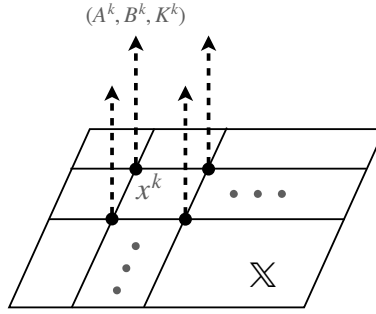


Figure 4. LPV models and control gains defined on a rectangular grid

(35) as a state-space model array defined on a finite grid domain, as shown in Figure 4. For each grid point  $x^k$ , there is a corresponding LTI system  $(A(x^k), B(x^k))$  which describes the dynamics of (35) where the scheduling variable  $x$  is held constant. For control of CMG, we use three grid points for each scheduling variable. Then, the pointwise LMI (12) is approximated by 243 LMIs of grid-dependent matrices  $Y^k \in \mathbb{R}^{5 \times 3}$  with  $k = 1, 2, \dots, 243$  and a dual metric  $W \in \mathbb{R}^{5 \times 5}$ . The control synthesis problem is solved by YALMIP [39] with the solver SDPT3 [40], which takes roughly 6.5s on MacBook Pro with Intel Core i5, 8GB memory and Matlab 2020a.

We determine the LPV control gain  $K_{\text{LPV}}(x)$  via linear interpolation of grid-dependent gain  $K^k = Y^k W^{-1}$ ,  $1 \leq k \leq 243$ . The tracking controller for the reference  $(x^*, u^*)$  takes the form of

$$\text{standard LPV: } u = u^* + K_{\text{LPV}}(x)(x - x^*). \quad (36)$$

For the two conditions of Theorem 1, the above realization only satisfies Condition C1.

**LPV-VCCM control.** We use the same design procedures of the standard LPV approach except the control realization. Here we choose the following controller

$$\text{LPV-VCCM: } u = k_{\text{LPV}}^{\text{ff}}(x^*, u^*, x) + K_{\text{LPV}}(x)(x - x^*), \quad (37)$$

where  $k_{\text{LPV}}^{\text{ff}}(x^*, u^*, x) := \mathcal{K}_m^{-1}[\mathcal{H}(x_1)\dot{x}_2^* + (\mathcal{C}(x_1, x_2) + \mathcal{F}_v)x_2^*]$ . Note that Conditions C1 - C2 hold for the above LPV-VCCM controller.

**NPV-VCCM control.** We choose the following NPV embedding of (33):

$$\dot{\chi} = A(x_1, \chi_2)\chi + B(x_1)\mu, \quad (38)$$

which explicitly considers the quadratic nonlinearity of  $x_2$  in the OM-1 dynamics. The nonlinearity of  $x_1$  is hidden in the external parameter so that the  $B$  matrix is independent of  $\chi$ , allowing a simpler formulation of (12) as it becomes independent of  $\mu$  [14].

The associated differential dynamics of (38) is

$$\dot{\delta}_\chi = \mathcal{A}(\sigma)\delta_\chi + B(\sigma)\delta_\mu, \quad (39)$$

where

$$\mathcal{A}(\sigma) = \begin{bmatrix} 0 & E \\ 0 & \mathcal{H}(x_1)^{-1}(2\mathcal{C}(x_1, \chi_2) + \mathcal{F}_v) \end{bmatrix}$$

with  $\sigma = (x_1, \chi_2)$  as the scheduling variable. For control synthesis, the operating range of  $\sigma$  is chosen to be the same as the LPV case. We solve (12) via grid-based approach to obtain the differential control gain  $K_{\text{NPV}}(x_1, \chi_2)$ . The control realization takes the form as follows:

$$\text{NPV-VCCM: } u = k_{\text{NPV}}^{\text{ff}}(x, x^*, u^*) + \left[ \int_0^1 K_{\text{NPV}}(x_1, \chi_2(s)) ds \right] (x - x^*) \quad (40)$$

with  $\chi_2(s) = (1 - s)x_2^* + sx_2$ , where the feed-forward term is chosen as

$$k_{\text{NPV}}^{\text{ff}}(x, x^*, u^*) := \mathcal{K}_m^{-1}[\mathcal{H}(x_1)\dot{x}_2^* + (\mathcal{C}(x_1, x_2^*) + \mathcal{F}_v)x_2^*]. \quad (41)$$

Note that the above realization satisfies both Conditions **C1** and **C2**. For online computation, the integral in (40) is approximated by

$$\int_0^1 K_{\text{NPV}}(x_1, \chi_2(s))ds \approx \frac{1}{N} \sum_{i=0}^{N-1} K_{\text{NPV}}(x_1, x_2^* + i(x_2 - x_2^*)/N) \quad (42)$$

where a large  $N$  can improve the accuracy but result in online computation delay. Here we found that  $N = 10$  can provide a good accuracy with minor control latency in this case.

#### 4.2. Under-actuated operating mode: OM-2

For the operating mode OM-2, the CMG becomes an under-actuated system as there is no motor torque acting on the gimbal A. The motion of the gimbal A is then mainly driven by the gyroscopic effect from the disk D and the gimbal C. Specifically, when the disk D satisfies  $\dot{q}_1 > 0$ , the motion of the gimbal C towards the direction  $q_2 > 0$  will generate a torque to drive the frame A towards the direction  $q_4 < 0$ , and vice versa. Thus, the variables  $q_2$  and  $q_4$  cannot be independently controlled, e.g. we cannot move  $(q_2, q_4)$  to the region  $\mathbb{R}_+^2$ . To avoid the difficulties of constructing an embedding satisfying Condition **C1** under such constraints, we exclude  $q_2$  from the state value and treat it as a scheduling variable. The dynamics of OM-2 can be represented by

$$\dot{x} = A(q_2, x_2)x + B(q_2)u := \begin{bmatrix} 0 & E \\ 0 & \mathcal{H}(q_2)^{-1}(\mathcal{C}(q_2, x_2) + \mathcal{F}_v) \end{bmatrix} \begin{bmatrix} x_1 \\ x_2 \end{bmatrix} + \begin{bmatrix} 0 \\ \mathcal{H}(q_2)^{-1}\mathcal{K}_m \end{bmatrix} u, \quad (43)$$

where  $x = (x_1, x_2)$  with  $x_1 = q_4$  and  $x_2 = (\dot{q}_1, \dot{q}_2, \dot{q}_4)$  is the state, and  $u = (i_1, i_2)$  the control input. It is important to note that the scheduling variable  $q_2$  is not a free external parameter as it is affected by the internal state  $\dot{q}_2$  of (43). Here  $\mathcal{H}, \mathcal{C}, \mathcal{F}_v$  are constructed by eliminating the 3rd row and column of the matrices  $H, C, F_v$  in (1), respectively, and  $\mathcal{K}_m$  is obtained by removing the 3rd row and 3-4th columns of  $K_m$ .

For performance design, we consider the following model:

$$\dot{x} = A(q_2, x_2)x + B(q_2)u + Dd, \quad z = \begin{bmatrix} W_1(x - x^*) \\ W_2(u - u^*) \end{bmatrix}, \quad (44)$$

with  $D = [0 \ 1 \ 0 \ 0]^\top$ , where  $d(t) \in \mathbb{R}$  is input perturbation. The weighting matrices is chosen as  $W_1 = \text{diag}(5, 0.1, 1, 4)$  and  $W_2 = \text{diag}(20, 10)$ , which will be explained later in Section 5.2. Similar to control design for OM-1, the rest of this section focuses on the Lyapunov design.

**Standard LPV control.** Here we consider the following LPV embedding of (43):

$$\dot{\chi} = A(q_2, x_2)\chi + B(q_2)\mu, \quad (45)$$

where the scheduling variable  $(q_2, x_2)$  is chosen to be within the range of  $q_2 \in [-\frac{\pi}{3}, \frac{\pi}{3}]$ ,  $\dot{q}_1 \in [30, 60]$  and  $\dot{q}_2, \dot{q}_4 \in [-1, 1]$ . We use the grid-based method to solve the pointwise LMI (12) with  $\lambda = 0.5$  and constant dual metric  $W$ . The control realization is similar to (36).

**LPV-VCCM control.** We use the same LPV embedding model and synthesis result from the standard LPV control design for OM-2. The corresponding LPV-VCCM controller can be written in the form of (37) but with a different feed-forward term

$$k_{\text{LPV}}^{\text{ff}}(x, x^*, u^*) := \mathcal{K}_m^\dagger[\mathcal{C}(q_2, x_2) + \mathcal{F}_v]x_2^*, \quad (46)$$

where  $\mathcal{K}_m^\dagger = (\mathcal{K}_m^\top \mathcal{K}_m)^{-1} \mathcal{K}_m^\top$  denotes the general inverse. Since OM-2 is under-actuated, it is easy to verify that Condition **C2** is not satisfied for any feed-forward term. The choice in (46) minimizes the residual term (31) so that CL performance loss as analyzed in Section 3.4 is reduced.

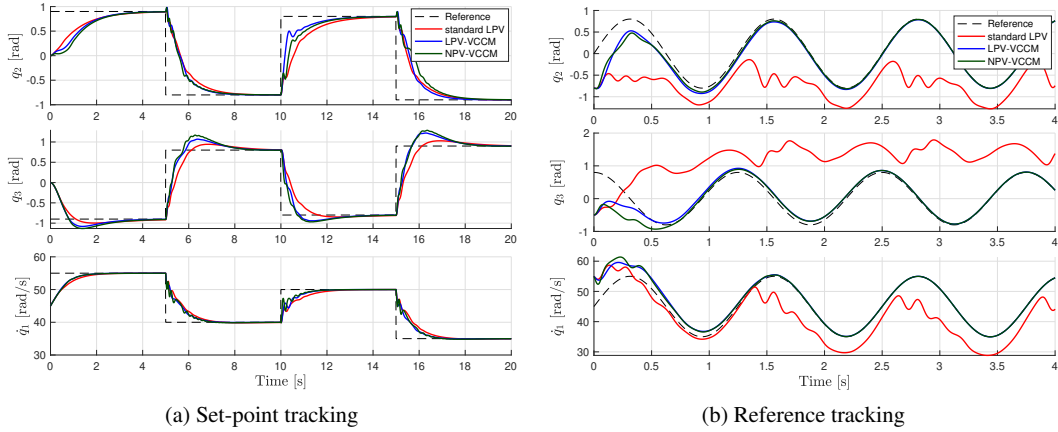


Figure 5. OM-1 simulation results of different tracking tasks with controllers obtained from (12).

**NPV-VCCM control.** We choose the trivial NPV embedding (i.e. the true system itself) of (43):

$$\dot{\chi} = A(q_2, \chi_2)\chi + B(q_2)\mu. \quad (47)$$

The reason for such choice is that Condition **C2** can be easily satisfied by simply using the feed-forward term  $\mu^* = u^*$ . The NPV-VCCM control realization can be expressed as

$$u = u^* + \left[ \int_0^1 K_{\text{NPV}}(q_2, \chi_2(s)) ds \right] (x - x^*), \quad (48)$$

where  $\chi_2(s) = (1-s)x_2^* + sx_2$ . Here the control gain  $K_{\text{NPV}}(q_2, \chi_2)$  is obtained by solving (12) with grid-based method subject to the same operation range as the standard LPV approach.

## 5. DISCUSSIONS ON SIMULATION AND EXPERIMENTAL RESULTS

### 5.1. Operating mode OM-1

We first compare the standard LPV, LPV-VCCM, and NPV-VCCM controllers obtained from Lyapunov design. The control tasks include tracking of set-points and a dynamic reference. The simulation results are depicted in Figure 5 where the LPV-VCCM and NPV-VCCM controllers have similar CL convergence rate as they both satisfy Conditions **C1** and **C2**. The standard LPV controller has similar convergence rate for set-point tracking but fails to track the dynamic reference. As analyzed in Section 3.4, this is mainly due to the violation of Condition **C2** for the standard LPV controller, which yields a residual term for the error dynamics as follows

$$\Delta(x, x^*)(x - x^*) = [\mathcal{H}(x_1) - \mathcal{H}(x_1^*)]\dot{x}_2^* + [\mathcal{C}(x_1, x_2) - \mathcal{C}(x_1^*, x_2^*)]x_2^*. \quad (49)$$

Note that  $\Delta$  is relatively small for set-points as  $\dot{x}_2^* = 0$ . The standard LPV controller can still have comparable performance to other controllers. However, it fails to converge to dynamic references as  $\Delta$  increases significantly with non-zero  $\dot{x}_2^*$ .

We also compare the controllers from performance design for tracking of dynamic references. In the simulation, neither exogenous input disturbance nor model uncertainty is considered. Figure 6(a) depicts the response for a periodic reference with frequency of 0.8Hz under large initial error. The experimental test contains both input disturbance (i.e. friction) and various type of model uncertainties (e.g., unmodeled velocity filter and input saturation). The response for a periodic reference with frequency of 0.2Hz and small initial error is shown in Figure 6(b). Both the simulation and experimental results reveal that the LPV-VCCM and NPV-VCCM controller have similar tracking performance while the standard LPV controller does not converge to the reference

Table II. Control performance comparison in OM-1: simulation - fast-varying reference and large initial error; experiment - slow-varying reference and small initial error.

Embedding	Gain bound $\alpha$	Realization	$J_{T=4}$ (simulation)	$J_{T=20}$ (experiment)
LPV	0.4585	standard LPV	446.3	32.8
		LPV-VCCM	19.9	19.5
NPV	0.4711	NPV-VCCM	19.3	7.7

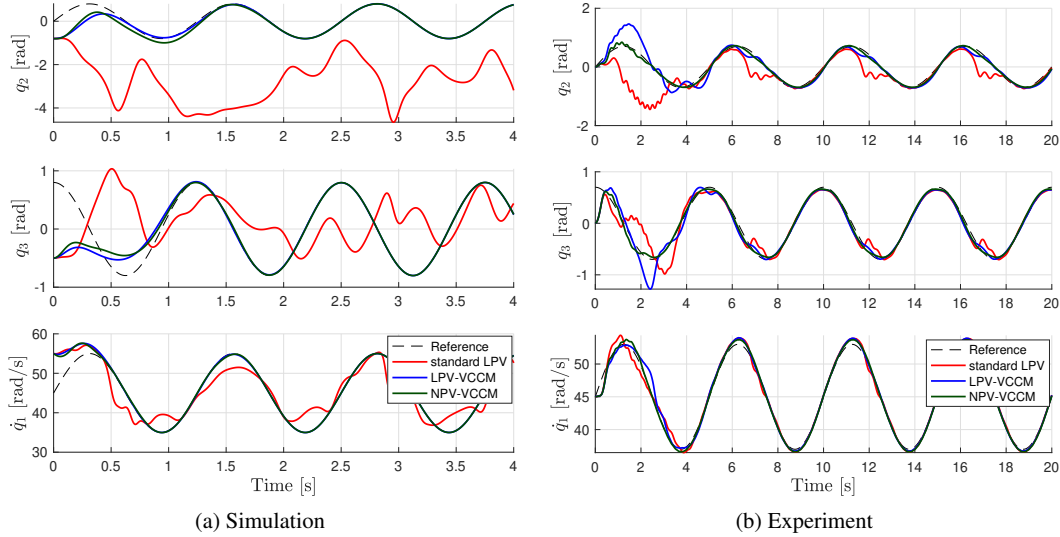


Figure 6. Comparison of controller obtained from (25) for OM-1: simulation - fast-varying reference and large initial error; experiment - slow-varying reference and small initial error.

trajectory. This also can be seen from the performance comparison in Table II. Note that for the standard LPV control design better performance can possibly be obtained using different weights and/or a different controller structure. However, the guarantees of converging towards the reference trajectory are always absent, while for the VCCM based designs one *does* have these guarantees.

### 5.2. Operating mode OM-2

We first simulate the CL responses of the standard LPV, LPV-VCCM and NPV-VCCM controllers obtained from Lyapunov design. Both small and large set-point are considered for the gimbal A, i.e.,  $|q_4^*| = 0.36\pi$  and  $|q_4^*| = 0.9\pi$ . As shown in Figure 7(a) where  $|q_4^*|$  is small, due to the violation of Condition C2, the convergence speed of the standard LPV and LPV-VCCM controllers is slower than the NPV-VCCM approach. The performance deterioration of LPV-VCCM is less severe due to the specific choice of the feed-forward input (46) where the residual term  $\Delta$  in (31) is minimized.

For moderate set-points  $|q_4^*| = 0.45\pi$ , the experimental result in Figure 8 reveals a significant performance loss for standard LPV controller compared with the VCCM approach. This is due to the small stability margin of the standard LPV approach and the large uncertainties presented in the experimental setting (i.e., friction force, unmodeled velocity filter and input saturation).

When  $|q_4^*|$  further increases, unstable CL behaviors are observed for both LPV-VCCM and NPV-VCCM controllers in simulation, as shown in Figure 7(b). The main cause is that the variable  $q_2$  exceeds the operation range for a large  $|q_4^*|$ . Those two controllers fail to keep  $q_2$  within its operation range because the Lyapunov design does not take  $q_2$  into account. Moreover, since the variables  $q_2$  and  $q_4$  are correlated, the LPV-VCCM and NPV-VCCM controllers give fast responses to  $q_4$  by pushing  $q_2$  towards the operation boundary, as shown in Figure 7(a).

Although the correlation between  $q_2$  and  $q_4$  causes stability issues, it also offers us a solution to address these issues via performance design. By choosing large weighting coefficients on  $q_4$  and  $\dot{q}_4$ ,

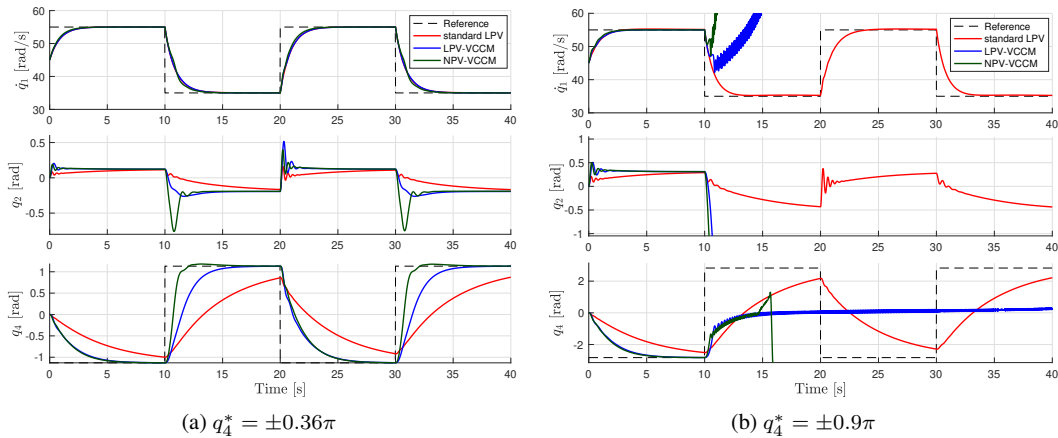


Figure 7. OM-2 simulation results of different set-points with controllers obtained from (12).

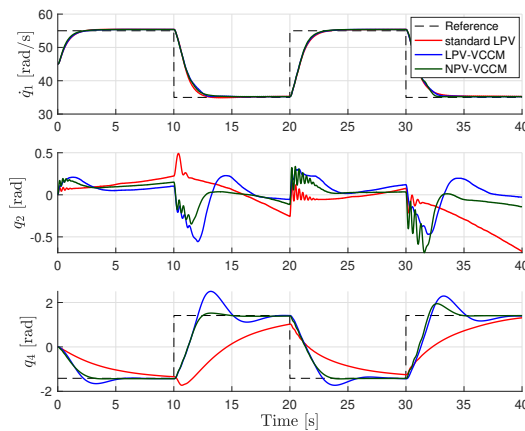


Figure 8. OM-2 experimental result of controllers obtained from (12) for moderate set-points.

it can help to keep  $q_2$  within its operation range. We observe acceptable simulation and experimental responses for the choice of  $W_1 = \text{diag}(5, 0.1, 1, 4)$  and  $W_2 = \text{diag}(20, 10)$ . Large  $W_2$  is used to cope with the uncertainty from input saturation.

The synthesis results (Table III) show that the universal  $\mathcal{L}_2$ -gain bounds for the LPV and NPV embedding are very close. Figure 9(a) shows that the standard LPV controller slightly outperforms the other two controllers in simulation. However, as shown in Figure 9(b), it leads to CL instability in the experiment where large uncertainties are presented. The loss of robustness is mainly due to the residual term in the Lyapunov analysis (32) for set-point tracking. This term is caused by violation of Condition C2 as analyzed in Section 3.4. Although the LPV-VCCM controller also violates this condition, it is more robust than the stand LPV controller as it uses a feed-forward term (46) that minimizes the residual term. For the NPV-VCCM controller which uses the same feed-forward term as the standard LPV approach, the difference is that it satisfies Condition C2 due to the choice of the particular NPV embedding (47). Then, its robust stability and performance can be guaranteed by Theorem 1 and (2) if  $q_2$  is kept within its operation range.

## 6. CONCLUSION

In this paper, we applied a virtual control contraction metric (VCCM) based nonlinear parameter-varying (NPV) approach to design state-feedback tracking controllers for two (both fully- and under-actuated) operation modes of a control moment gyroscope. This approach includes three steps: 1)



Table III. Performance comparison with different embedding models and realizations for OM-2.

Embedding	Gain bound $\alpha$	Realization	$J_{T=40}$ (simulation)	$J_{T=40}$ (experiment)
LPV	1.2035	standard LPV	$2.1314 \times 10^4$	unstable
		LPV-VCCM	$2.6816 \times 10^4$	$1.0901 \times 10^5$
NPV	1.2094	NPV-VCCM	$2.8506 \times 10^4$	$1.2753 \times 10^5$

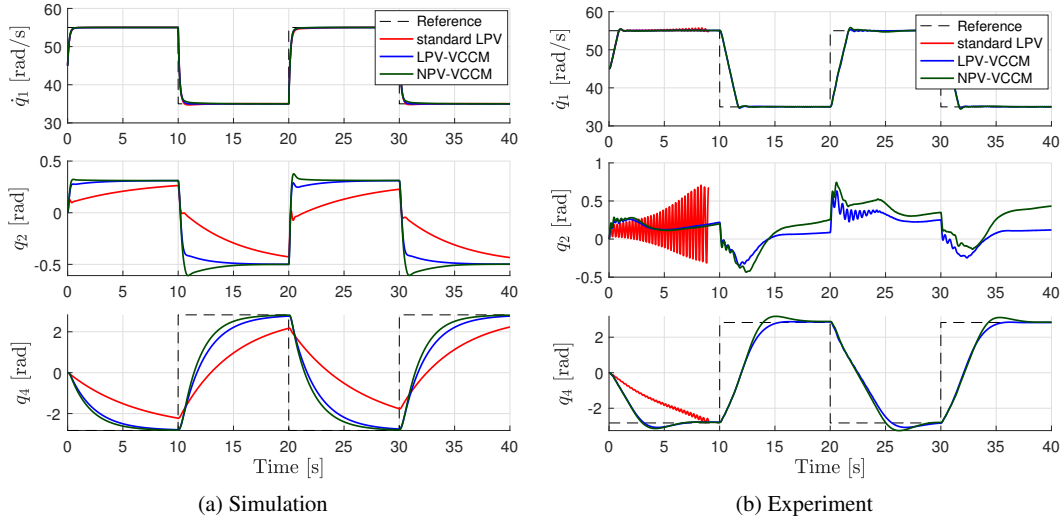


Figure 9. OM-2 set-point tracking comparison of controllers obtained from (25).

choose a NPV embedding, 2) search for a VCCM and 3) realize the controller back into the original state/input space. Since the NPV embedding is non-unique but essential for control synthesis and realization, we provided two conditions for the choice of NPV models: **(C1)** the NPV virtual system is universally stabilizable, and **(C2)** the desired reference is an admissible state trajectory of the NPV embedded system. Condition **C1** can be easily verified via a convex control synthesis formulation similar to the conventional LPV approach. Condition **C2** determines whether a control realization can provide closed-loop stability and performance guarantees or not. As shown in simulation and experimental comparisons, the standard LPV control realization does not ensure closed-loop stability and performance as it does not satisfy Condition **C2** while the VCCM based realization addresses this issue by utilizing additional freedom in feed-forward control design. [Future works include dynamic controller realizations to relax Condition C2.](#)

## REFERENCES

1. Tóth R. *Modeling and Identification of Linear Parameter-Varying Systems*. Lecture Notes in Control and Information Sciences, Vol. 403, Springer: Heidelberg, 2010.
2. Apkarian P, Gahinet P. A convex characterization of gain-scheduled  $h_\infty$  controllers. *IEEE Transaction Automatic Control* 1995; **40**:853–864.
3. Scherer CW. Mixed  $H_2/H_\infty$  Control for Linear Parametrically Varying Systems. *Proceedings of of the 34th IEEE Conferene on Decision & Control*, vol. 3, 1995; 3182–3187.
4. Wu F, Dong K. Gain-scheduling control of lft systems using parameter-dependent lyapunov functions. *Automatica* 2006; **42**(1):39–50.
5. Xie X, Yue D, Peng C. Relaxed real-time scheduling stabilization of discrete-time takagi–sugeno fuzzy systems via an alterable-weights-based ranking switching mechanism. *IEEE Transactions on Fuzzy Systems* 2018; **26**(6):3808–3819.
6. Cai X, Liu Y, Zhang W. Control design for a class of nonlinear parameter varying systems. *International Journal of Systems Science* 2015; **46**(9):1638–1647.
7. Sala A, Ariño C, Robles R. Gain-Scheduled Control via Convex Nonlinear Parameter Varying Models. *Proc. of the 3rd IFAC Workshop on Linear Parameter Varying Systems*, Eindhoven, The Netherland, 2019; 70–75.

8. Rotondo D, Witczak M. Analysis and design of quadratically bounded QPV control systems. *3rd IFAC Workshop on Linear Parameter-Varying Systems*, Eindhoven, The Netherlands, 2019; 76–81.
9. Mohammadpour Velni J, Scherer CW. *Control of Linear Parameter Varying Systems with Applications*. Springer Science & Business Media, 2012.
10. Hoffmann C, Werner H. A survey of linear parameter-varying control applications validated by experiments or high-fidelity simulations. *IEEE Transactions on Control System Technology* 2015; **23**(2):416–433.
11. Scorletti G, Fromion V, De Hillerin S. Toward nonlinear tracking and rejection using LPV control. *Proc. 1st IFAC Workshop on Linear Parameter Varying Systems, Grenoble, France*, 2015; 13–18.
12. Koelewijn PJW, Tóth R, H N. Linear parameter-varying control of nonlinear systems based on incremental stability. *3rd IFAC Workshop on Linear Parameter-Varying Systems*, Eindhoven, The Netherlands, 2019; 38–43.
13. Koelewijn PJW, Sales Mazzocante G, Tóth R, Weiland S. Pitfalls of Guaranteeing Asymptotic Stability in LPV Control of Nonlinear Systems. Accepted to the European Control Conference, 2020.
14. Manchester IR, Slotine JJE. Control contraction metrics: Convex and intrinsic criteria for nonlinear feedback design. *IEEE Transaction Automatic Control* 2017; **62**(6):3046–3053.
15. Sontag ED. A Lyapunov-like characterization of asymptotic controllability. *SIAM Journal on Control and Optimization* 1983; **21**(3):462–471.
16. Manchester IR, Slotine JJE. Robust control contraction metrics: A convex approach to nonlinear state-feedback  $H_\infty$  control. *IEEE Control System Letter* 2018; **2**(3):333–338.
17. Lohmiller W, Slotine JJE. On contraction analysis for non-linear systems. *Automatica* 1998; **34**:683–696.
18. Forni F, Sepulchre R. A differential Lyapunov framework for contraction analysis. *IEEE Transactions Automatic Control* 2014; **3**(59):614–628.
19. Wang R, Tóth R, Manchester IR. Virtual control contraction metrics: Convex nonlinear feedback design via behavioral embedding. *arXiv preprint arXiv:2003.08513* 2020; .
20. Wang W, Slotine JJE. On partial contraction analysis for coupled nonlinear oscillators. *Biological cybernetics* 2005; **92**(1):38–53.
21. Joffroy J, Fossen TI. A tutorial on incremental stability analysis using contraction theory. *Modeling, Identification and Control* 2010; **31**(3):93–106.
22. Manchester IR, Tang JZ, Slotine JJE. Unifying robot trajectory tracking with control contraction metrics. *Robotics Research*. Springer, 2018; 403–418.
23. Reyes-Báez R, van der Schaft A, Jayawardhana B, Pan L. A family of virtual contraction based controllers for tracking of flexible-joints port-hamiltonian robots: Theory and experiments. *International Journal of Robust and Nonlinear Control* 2020; **30**(8):3269–3295.
24. van de Wouw N, Pastink H, Heertjes MF, Pavlov AV, Nijmeijer H. Performance of convergence-based variable-gain control of optical storage drives. *Automatica* 2008; **44**(1):15–27.
25. Van Loon S, Hunnekens B, Simon A, van de Wouw N, Heemels W. Bandwidth-on-demand motion control. *IEEE Transactions on Control Systems Technology* 2017; **26**(1):265–273.
26. Perez T, Steinmann PD. Analysis of ship roll gyro stabiliser control. *IFAC Proceedings Volumes* 2009; **42**(18):310–315.
27. Lappas V, Steyn W, Underwood C. Design and testing of a control moment gyroscope cluster for small satellites. *Journal of Spacecraft and Rockets* 2005; **42**(4):729–739.
28. Gurrisci C, Seidel R, Dickerson S, Didziulis S, Frantz P, Ferguson K. Space station control moment gyroscope lessons learned. *Proceedings of the 40th Aerospace Mechanisms Symposium*, NASA/CP-2010-216272, Kennedy Space Center, 2010.
29. Reyhanoglu M, van de Loo J. State feedback tracking of a nonholonomic control moment gyroscope. *IEEE Conference on Decision and Control*, IEEE, 2006; 6156–6161.
30. Abbas HS, Ali A, Hashemi SM, Werner H. Lpv state-feedback control of a control moment gyroscope. *Control Engineering Practice* 2014; **24**:129–137.
31. Bloemers TAH, Tóth R. Equations of motion of a control moment gyroscope. Technical Report, Eindhoven University of Technology, 2019.
32. van Berkel M. Explicit solution of the odes describing the 3-dof control moment gyroscope. Technical Report, Eindhoven University of Technology, 2019.
33. Parrilo PA. Semidefinite programming relaxations for semialgebraic problems. *Mathematical Programming* 2003; **96**(2):293–320.
34. Tóth R, Willems JC, Heuberger PS, Van den Hof PM. The behavioral approach to linear parameter-varying systems. *IEEE Transactions on Automatic Control* 2011; **56**(11):2499–2514.
35. Leung K, Manchester IR. Nonlinear stabilization via control contraction metrics: A pseudospectral approach for computing geodesics. *Proceedings American Control Conference, Seattle, WA*, 2017; 1284–1289.
36. Wang R, Manchester IR. Continuous-time dynamic realization for nonlinear stabilization via control contraction metrics. Accepted by American Control Conference, 2020.
37. Dullerud GE, Paganini F. *A course in robust control theory: A convex approach*, vol. 36. Springer Science & Business Media, 2013.
38. Wu F. Control of Linear Parameter Varying Systems. PhD Thesis, University of California at Berkeley 1995.
39. Löfberg J. YALMIP: A toolbox for modeling and optimization in MATLAB. *IEEE International Symposium on Computer Aided Control Systems Design*, 2004; 284–289.
40. Toh KC, Todd MJ, Tütüncü RH. SDPT3 – A Matlab software package for semidefinite programming, version 1.3. *Optimization Methods and Software* 1999; **11**(1-4):545–581.